

Available online at [www.sciencedirect.com](http://www.sciencedirect.com)

ScienceDirect

journal homepage: [www.elsevier.com/locate/he](http://www.elsevier.com/locate/he)

# Achieving high-efficiency hydrogen production using planar solid-oxide electrolysis stacks

Qingshan Li, Yifeng Zheng, Wanbing Guan, Le Jin, Cheng Xu<sup>\*</sup>,  
Wei Guo Wang<sup>\*\*</sup>

Ningbo Institute of Material Technology & Engineering, Chinese Academy of Sciences, 1219 Zhongguan West Road, Ningbo 315201, PR China

## ARTICLE INFO

### Article history:

Received 15 January 2014

Received in revised form

8 May 2014

Accepted 10 May 2014

Available online 11 June 2014

### Keywords:

Solid oxide electrolysis cell

Hydrogen production

System efficiency

High-temperature electrolysis

## ABSTRACT

Steam electrolysis in solid oxide electrolysis cells (SOECs) is considered as an effective method to achieve high-efficiency hydrogen production. In the present investigation, samples of 1-cell, 2-cell and 30-cell SOEC stacks were tested under electrolysis of steam to give a practical evaluation of the SOEC system efficiency of hydrogen production. The samples were tested at 800 °C under various operating conditions up to 500 h without significant degradation, and obtained steam conversion rates of 12.4%, 23% and 82.2% for the 1-cell, 2-cell and 30-cell stacks, respectively. System efficiencies of hydrogen production were calculated for the samples based on their real performance. A maximum efficiency value of 52.7% was achieved in the 30-cell stack.

Copyright © 2014, Hydrogen Energy Publications, LLC. Published by Elsevier Ltd. All rights reserved.

## Introduction

Hydrogen is considered as a promising energy carrier due to increasing concern about the depletion of fossil fuels and greenhouse gas emission. At present, hydrogen is produced predominately from fossil fuels; around 96% hydrogen is produced by steam reforming of natural gas [1,2]. It is thus imperative to develop environment-friendly and economically viable technologies for large-scale hydrogen production. Extensive investigations have been conducted to explore the methods of obtaining hydrogen in sustainable and clean manner, such as by photocatalytic water-splitting [3], gasification of biomass [4], solar thermochemical water-splitting [5], or water electrolysis driven by solar cells or wind turbines [6]. Among all the above technologies, water electrolysis

is featured by its high efficiency and practicability for large-scale hydrogen production.

Steam electrolysis in solid oxide electrolysis cells (SOECs) has been a subject of increasing interest in recent years for its high efficiency and feasibility to be coupled with renewable resources [7–15]. SOEC is essentially the reverse of solid oxide fuel cell (SOFC); it produces hydrogen by splitting steam at the cathode (hydrogen electrode) while oxygen ions resulted from steam splitting transport through the electrolyte to form oxygen at the anode (oxygen electrode). SOECs work at high temperatures of 500–800 °C, which distinguishes it from conventional electrolyzers such as alkaline electrolyzers which work in the temperature range of 100–150 °C. Since water electrolysis is increasingly endothermic with temperature, SOECs can utilize effectively the heat available at these higher temperatures from nuclear energy or renewable energy

<sup>\*</sup> Corresponding author. Tel.: +86 574 8668 5139; fax: +86 574 8669 5470.

<sup>\*\*</sup> Corresponding author. Tel.: +86 574 8791 1363; fax: +86 574 8669 5470.

E-mail addresses: [xucheng@nimte.ac.cn](mailto:xucheng@nimte.ac.cn) (C. Xu), [wgwang@nimte.ac.cn](mailto:wgwang@nimte.ac.cn) (W.G. Wang).

<http://dx.doi.org/10.1016/j.ijhydene.2014.05.070>

0360-3199/Copyright © 2014, Hydrogen Energy Publications, LLC. Published by Elsevier Ltd. All rights reserved.

sources such as solar thermal energy and wind turbine. In the mean time, SOECs can reduce the amount of electrical energy necessary for the production of hydrogen. Therefore, the SOEC system is viable to achieve higher overall efficiency.

Recent researches on SOECs have shown the potential of effective hydrogen production via SOECs [16–20]. Herring et al. at the Idaho National Engineering and Environmental Laboratory (INEEL) performed experiments in SOEC mode for hydrogen production using a 10-cell planar solid-oxide stack produced by Ceramtec, Inc., and obtained favorable results in comparison with a three-dimensional computational fluid dynamics (CFD) model they proposed [16]. Ebbesen et al. [17] also showed long-term steam electrolysis was feasible without notable degradation in their 6–10 cell planar SOEC stacks. Kim et al. [18] reported a hydrogen production rate of 4.1 L h<sup>-1</sup> for the operation of a 3-cell flat-tubular SOEC stack.

System efficiency for hydrogen production is an important parameter for SOEC systems, but only a limited number of studies involved SOEC system efficiency calculations. Based on the first law of thermodynamics, the SOEC system efficiency can be described by:

$$\eta = \frac{N_{\text{H}_2, \text{out}} \cdot \text{HHV}}{E + Q_{\text{H}_2\text{O}} + Q_{\text{cell}}} \quad (1)$$

where  $N_{\text{H}_2, \text{out}}$  is the outlet flow rate of H<sub>2</sub>, HHV is the higher heating value of H<sub>2</sub>,  $E$  is the electric energy input,  $Q_{\text{H}_2\text{O}}$  is the thermal energy input to heat up H<sub>2</sub>O and  $Q_{\text{cell}}$  is the heat demand for the electrolysis reaction [19]. Ni et al. [19] developed a thermodynamic–electrochemical model to simulate the hydrogen production by a SOEC plant and conducted energy and exergy analysis based on a SOEC cell with an active area of 1 m<sup>2</sup>. They found the difference between energy efficiency and exergy efficiency is small at higher temperatures. In contrast, the energy efficiency and exergy efficiency of a low-temperature electrolysis plant differ noticeably as the considerable waste heat dissipating to the environment contains little exergy at low temperatures. Wang et al. [20] estimated the efficiency of a hydrogen production system operating at a capacity of 300 Nm<sup>3</sup> h<sup>-1</sup> on the basis of the electrolytic characteristics of a tubular cell, and showed the system efficiency could reach a higher heating value (HHV standard) of 98% due to the effective recovery of thermal energy from exhaust gas. Zhang et al. [21] showed the overall system efficiency could achieve from 44% to 56% at the temperature of 650–850 °C when the SOEC system was coupled directly with nuclear reactors. These values were calculated taking account of electrical power as secondary power, and were much lower than the SOEC system efficiency [19,20]. However, the values reported by Zhang et al. [21] were much higher than the system efficiencies for the alkaline electrolysis system (~25%) and the solid polymer electrolysis system (~35%) [22]. All above research investigated the hydrogen production efficiency for SOEC system is based on performance of a single cell. In practice, the real SOEC system works on the basis of SOE stacks and its efficiency is influenced by not only cell performance but also interconnects, sealants and other stack factors. These stack factors will lead to a large deviation of the real system efficiency from current calculations. However, systematic studies about the influence of SOEC stacks on system efficiency remain lacking. Recently

Kim et al. [18] obtained a total electric efficiency of 97.61% using a 3-cell tubular electrolysis stack, but this efficiency was essentially faradic efficiency which took no account of the thermal energy demand for the system.

The aim of this paper is to investigate the hydrogen production efficiency of SOEC systems based on planar-type SOEC stacks. In the present study, we have evaluated the hydrogen production efficiency based on the performance of a planar cathode-supported SOEC 1-cell, 2-cell and 30-cell electrolysis stacks. A maximum operation time up to 500 h has been achieved for the efficiency calculation, which makes our efficiency calculation more solid and reliable.

## Experimental

### Sample preparing

The investigation was conducted using three SOEC stack samples made of 1 cell, 2 cells and 30 cells. The cells used for sample preparation were planar cathode-supported Ni-YSZ/YSZ/LSM-YSZ SOEC cells manufactured at the Division of Fuel Cell and Energy Technology in the Ningbo Institute of Material Technology and Engineering, Chinese Academy of Sciences (NIMTE, CAS). A 400 μm thick substrate of Ni-YSZ was tape cast as the support, and a 10 μm thick electrode of Ni-YSZ and a 10 μm thick electrolyte of 8YSZ were sprayed onto the support substrate followed by sintering at 1200 °C. A 30–40 μm thick electrode of 50 wt% La<sub>0.75</sub>Sr<sub>0.25</sub>MnO<sub>3</sub> (LSM) and 50 wt% YSZ was then screen printed on the electrolyte and fired at 1225 °C. The total area of the cell was 10 × 10 cm<sup>2</sup> and the active area of the cell was 63 cm<sup>2</sup>. Details of the cell preparation can be found elsewhere [23].

The SOEC stacks were made of SOEC cells, interconnects of SUS430 ferritic stainless steel and glass sealants. In the stack, the metallic interconnect was etched to create co-flow gas channels. To prevent high-temperature oxidation, the LSM–YSZ electrode side of the interconnect plate was coated with a dense LSM layer by plasma spraying. Porous nickel foam was placed on the Ni–YSZ electrode side of the interconnect as the current collecting layer whereas an extra layer of LSM of approximately 75 μm were coated on the original LSM–YSZ electrode side to improve the output performance of the stack and individual cells. Other parameters of the stacks are listed elsewhere [24].

### Experimental apparatus and procedure

A newly developed testing system was used for SOEC testing. As shown in Fig. 1, the system contained a gas/steam mixing and preheating facility (including a peristaltic pump and a gas/steam mixer), a gas mixture transporting line with line heater, an electrochemical testing rig and a condenser. During the test, water flew into the mixer and evaporates while mixing with the carrier gas which in our scenario was hydrogen. The mixture gases of steam and hydrogen were then brought to the hydrogen electrode of the sample through the heated transportation gas line. In this system, the flow rate of water was controlled by the pump with an accuracy of ±0.5%, therefore a relative stable steam-to-H<sub>2</sub> ratio can be

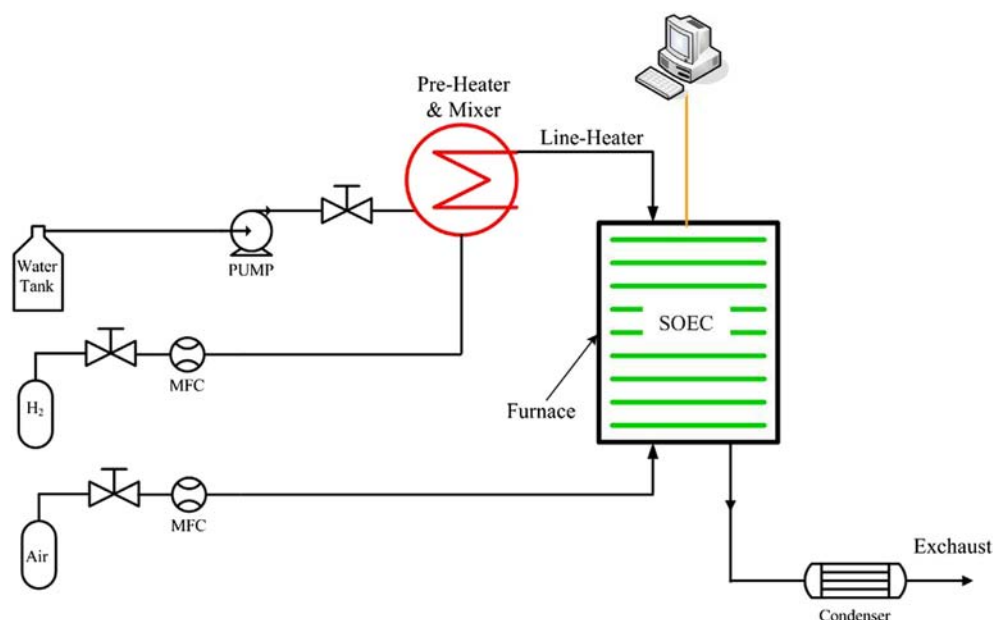


Fig. 1 – Schematic diagram of the HTE system.

achieved during the testing. A flow meter was placed after the condenser in order to evaluate the output gas quantitatively, which was crucial for the calculation of steam conversion rate and system efficiency in the present study.

Prior to the testing, the samples were assembled on the testing rig in the furnace. Fig. 2 shows an exploded view of the single cell testing assembly. For comparison, the samples of 1-cell, 2-cell and 30-cell stacks adopted a repeating cell structure of interconnect/cell/interconnect as shown in Fig. 2. Ag meshed sheets were placed between the interconnect plate and top/base plate to give a better contact. Leads of Ni–Cr alloy and Pt were placed at the cathode and anode side of the samples, respectively, for voltage measurements

After assembly, the samples were heated to 800 °C with a rate of 1 °C min<sup>-1</sup> and remained at 800 °C for 1 h. N<sub>2</sub> of commercial purity was fed into the samples for protection during heating. A certain amount of external pressure was loaded on the sample for several seconds using a loading facility. The loading facility was specifically designed for external loading and the load cell had a capacity up to 500 kg. Then hydrogen was fed in the cathode of the samples while air was fed in the anode, respectively. The flow rate of each gas was controlled by separate flow meter. Each sample was reduced for at least 2 h to achieve a complete reduction of NiO at the cathode before charging/discharging tests [23].

The electrolysis test was conducted by feeding a mixture gas of steam and hydrogen. The electrolysis performance was examined under different H<sub>2</sub>O/H<sub>2</sub> ratios and current density values. The real-time curves of polarization (*I*–*V*) and voltage (*V*–*t*) were recorded by a DC stabilized power supply system (NB M&C Technology Co. Ltd.). Impedance spectroscopy was measured via the four-wire method by a ZAHNER elektrik IM6ex electrochemical workstation in galvanostatic mode between 20 mHz and 10 kHz. Post-mortem analysis was conducted using a HITACHI-S 4800 scanning electron microscopy (SEM).

## Results and discussion

### Electrolysis performance under different operating conditions

In the electrolysis test, various ratios of steam to hydrogen were used. Fig. 3 shows the recorded polarization curves (*I*–*V*) for the samples of 1-cell, 2-cell and 30-cell stacks tested at 800 °C. All samples exhibit stable electrolysis performance at

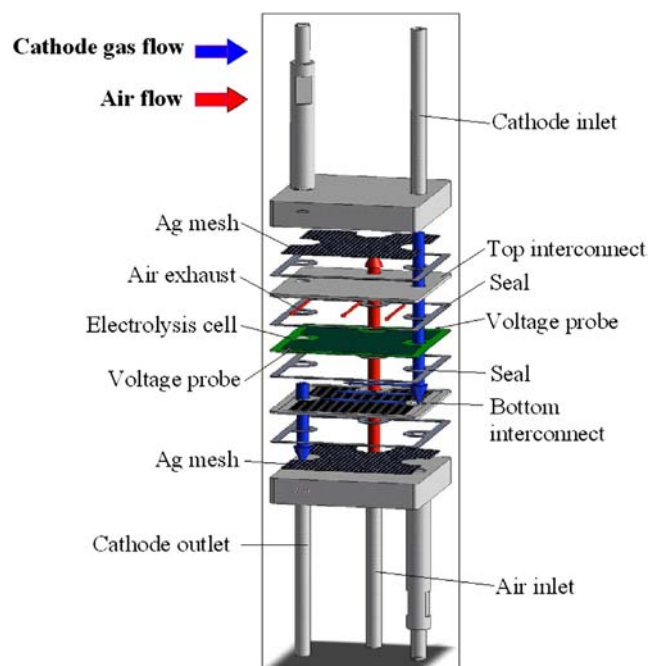


Fig. 2 – Schematic diagram of the electrolysis cell assembling.

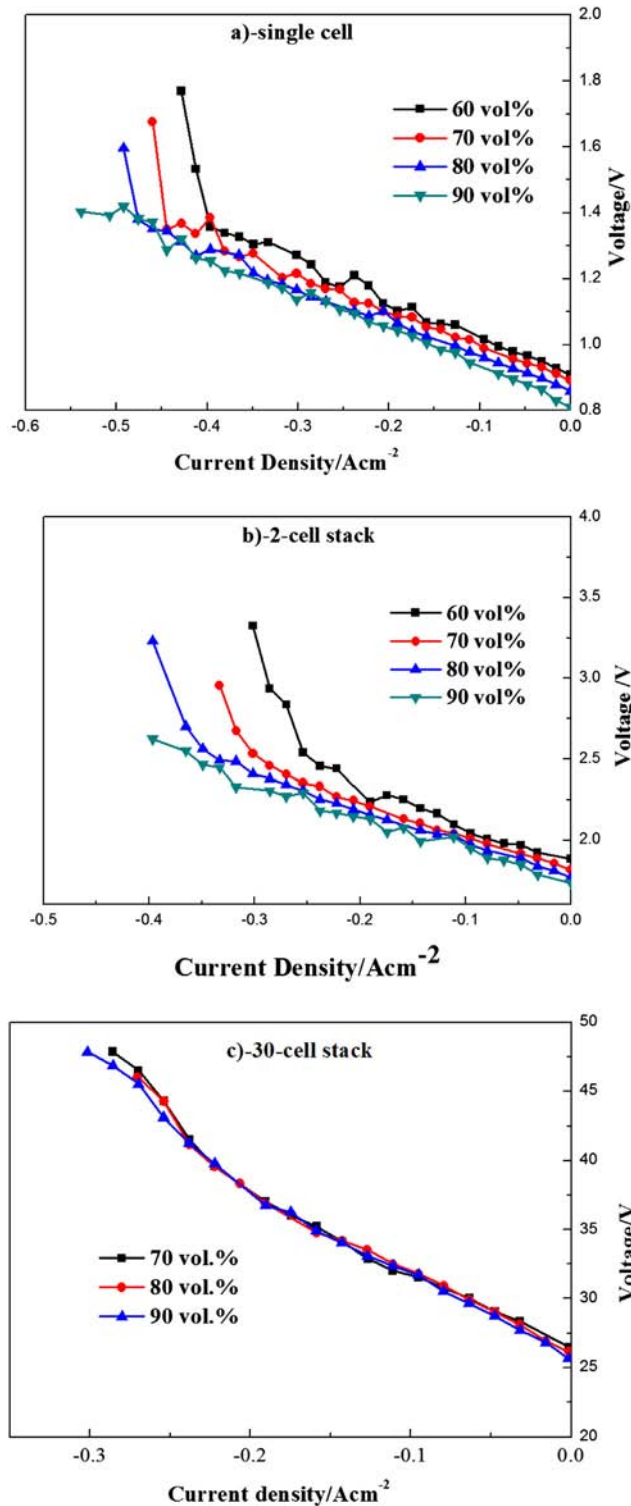


Fig. 3 – I–V curves at different steam contents for stacks (a) 1-cell; (b) 2-cell; (c) 30-cell.

low current densities (typically  $i < 0.3\text{--}0.4 \text{ A cm}^{-2}$ ), but show a rapid increase of area specific resistance (ASR) when the testing current densities go beyond  $0.3\text{--}0.4 \text{ A cm}^{-2}$ . This increase in ASR is more significant for the samples of 1-cell and 2-cell stacks when testing at a relatively low steam content ( $<70 \text{ vol}\% \text{ H}_2\text{O}$ ). The 30-cell stack shows rather similar

polarization curves for varying steam contents. This may be because the testing current densities for the 30-cell stack are below  $0.3 \text{ A cm}^{-2}$ , lower than the critical current density for 1-cell and 2-cell stacks to degrade.

More detailed analysis of polarization was conducted on the samples of 1-cell and 2-cell stacks using electrochemical impedance spectroscopy (EIS). All the EIS tests were conducted at open circuit voltage (OCV) and typical spectra for the 1-cell and 2-cell stacks are shown in Fig. 4. All the obtained spectra were fitted into the equivalent circuit model consisting of one standard resistor ( $R$ ) in series with two R-CPE (constant phase element) units. It can be seen that the steam content has little effect on the ohmic resistance of the samples ( $R_S$ ), but has a significant impact on the polarization resistance ( $R_P$ ). The  $R_P$  decreases with the increase of steam content until the steam content of 80%. When the steam content further increases to 90 vol%, the  $R_P$  rises. This tendency can be observed for both 1-cell and 2-cell stack. The reduction of  $R_P$  up to 80% steam content may be because of the increase of the reactant concentration, while the increase of  $R_P$  with further increase of steam content to 90% could possibly lead to local oxidation of Ni. Dasari et al. [26] recently obtained similar EIS results when they tested symmetrical Ni-YSZ/YSZ/Ni-YSZ cells in the mode of SOEC under various

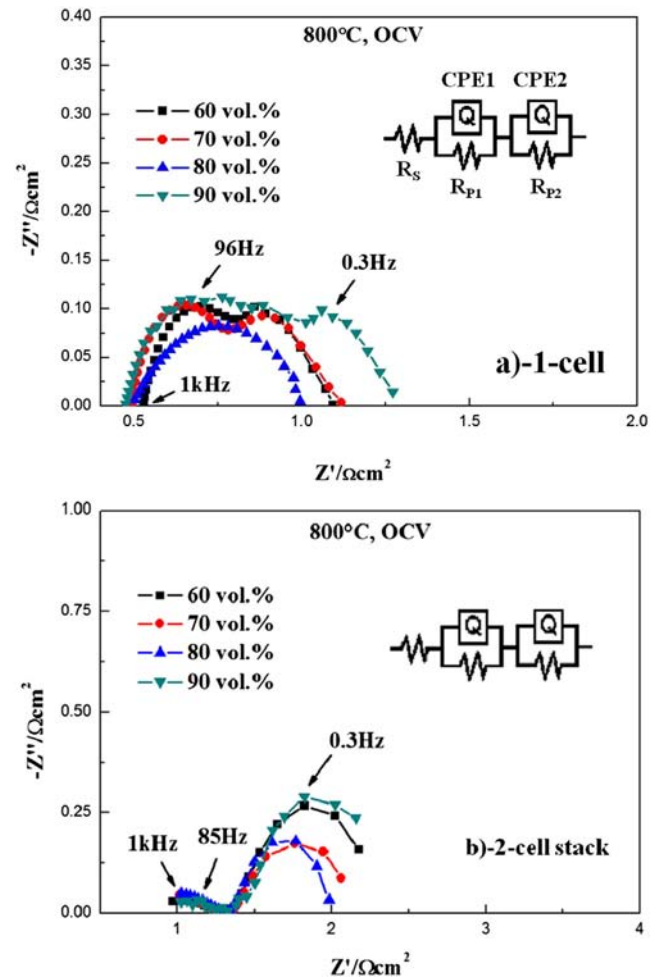


Fig. 4 – The impedance spectra tested at various steam contents for stacks of (a) 1-cell and (b) 2-cell.

steam contents (35%–60%), but they discovered an optimum steam content of 50%, which is much lower than our optimum steam content value. This may be because their symmetrical cells could be more sensitive to steam content.

The EIS results are summarized in Table 1. It is noted that the  $R_S$  and  $R_P$  for the 2-cell stack are larger than 2 times of the  $R_S$  and  $R_P$  values for the single cell. This is a consequence of the contact resistance and the interconnector resistance in the stack. This disproportion in resistance further leads to the disproportion between the system efficiency of the single cell and that of the 2-cell stack.

#### Electrolysis durability under different testing conditions

Electrolysis durability of the samples was investigated in order to make the system efficiency calculation more practical. Fig. 5 shows the long-term durability of 1-cell, 2-cell and 30-cell stacks. As shown in Fig. 5a, the cell was tested in SOFC mode during the first 30 h of the testing, and then was tested under electrolysis at various current density at 800 °C with a steam content of 80 vol% up to 120 h. In spite of the current density variation during the test, the voltage variation at each current density is negligible except some slight fluctuation due to the instable water supply. In the 2-cell stack test (Fig. 5b), the electrolysis voltages of the two unit cells nearly coincide with each other, which indicates the consistency of their performance during stack performance measurements. The 30-cell stack was also tested in SOEC mode up to 500 h as shown in Fig. 5c. The operating current density was changed to 0.2 A cm<sup>-2</sup> to keep consistency with other samples for the system efficiency investigation. The ASR (area specific resistance) is calculated via:  $ASR (\Omega \text{ cm}^2) = (E-OCV)/i$ , where  $E$  is the electrolysis voltage and  $i$  is the current density. According to Fig. 5, the ASR for the 1-cell, 2-cell and 30-cell stacks are 1.43  $\Omega \text{ cm}^2$ , 2.698  $\Omega \text{ cm}^2$  and 37.79  $\Omega \text{ cm}^2$ , respectively. Apparently, the ASR of the 30-cell stack is much less than 30 times of the ASR of the single cell, or 15 times of that of the 2-cell stack.

Further inspection of the degradation of the stacks during electrolysis test can be seen in Fig. 6, where the  $I$ – $V$  curves before and after electrolysis test are shown for comparison. Both the 1-cell and 2-cell stacks were tested at various current densities and operated for at least 10 h at each current density. No remarkable change of the slope can be observed, especially at low current densities. A slight increase of the slope was observed for the 1-cell stack testing at high current densities, indicating some deterioration of the cell during testing. The 30-cell stack was tested at a current density of 0.15 A cm<sup>-2</sup> for ~500 h and then tested at 0.2 A cm<sup>-2</sup> for ~20 h. The OCV of the

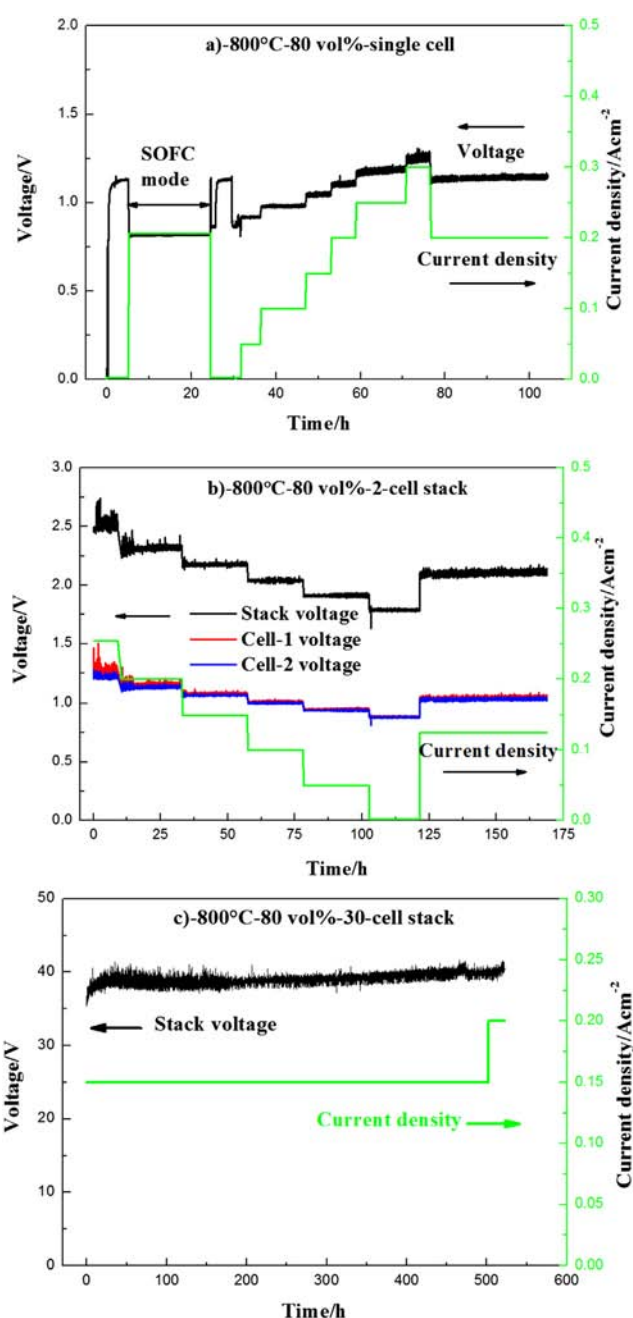


Fig. 5 – Long-term durability tests for stacks of (a) 1-cell; (b) 2-cell; (c) 30-cell.

30-cell stack remained the same during the entire operation indicating no significant sealing deterioration, but the ASR of the stack increased when operated in SOEC mode. This increase of ASR may be due to the degradation of the stack after 500-h operation at 0.15 A cm<sup>-2</sup>, and the increase of ASR with the increase of current density may be the direct effect of the degraded stack.

Fig. 7 shows impedance spectra for the 1-cell and 2-cell stacks before and after electrolysis test. All the impedance spectra were recorded at OCV. The results show a stable  $R_S$  and a varied  $R_P$  for the stacks after tested under different current densities, which can be referred to the variation of the slope in the  $I$ – $V$  curves.

Table 1 – EIS results at various steam content for the single cell and 2-cell stack.

Steam content	Single cell		2-cell stack	
	$R_S/\Omega \text{ cm}^2$	$R_P/\Omega \text{ cm}^2$	$R_S/\Omega \text{ cm}^2$	$R_P/\Omega \text{ cm}^2$
60 vol.%	0.507	1.074	1.054	2.205
70 vol.%	0.496	1.071	1.071	2.205
80 vol.%	0.504	0.926	1.068	1.890
90 vol.%	0.500	1.286	1.050	2.520

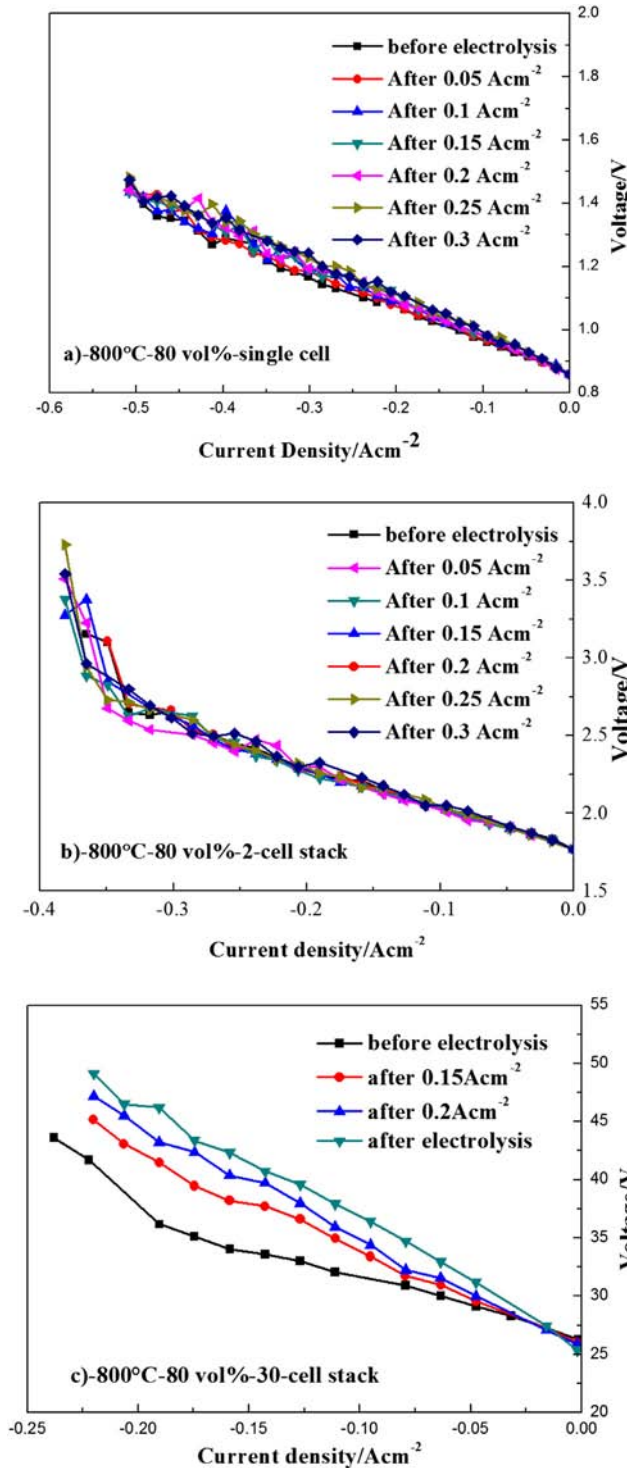


Fig. 6 – I–V curves before and after electrolysis for stacks of (a) 1-cell; (b) 2-cell; (c) 30-cell.

Post-mortem examination was conducted using stacks disassembled from the testing rig. Fig. 8 shows the cross-sectional microstructure characterization for the cell in the 1-cell stack before and after electrolysis test. No significant change in microstructure can be observed in the cell before and after electrolysis. The agglomeration of Ni particle in the cathode side is negligible even for the sample exposed to 90% steam content. Fig. 9 shows the cross-sectional

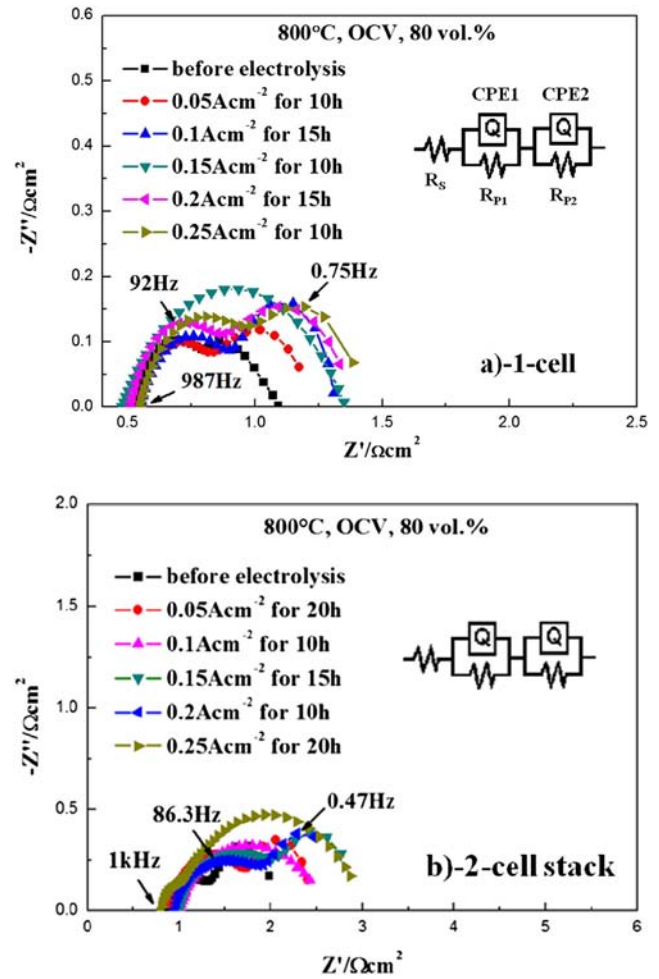


Fig. 7 – The impedance spectra tested before and after electrolysis for stacks of (a) 1-cell and (b) 2-cell.

microstructure for the bottom cell in the 2-cell stack before and after electrolysis. Cavities with considerable sizes can be observed in the interface between the oxygen electrode and electrolyte after electrolysis, but no significant detachment can be detected. Fig. 10 shows the cross-sectional microstructure for the cell-2 (top cell) in the 2-cell stack. Samples (b), (c) and (d) were selected in the area close to the cathode inlet, cathode outlet and air inlet, respectively. No significant degradation of microstructure can be inspected in the top cell.

In summary, all cells in the samples of the 1-cell and 2-cell stacks exhibit little degradation after electrolysis, which is consistent with the performance we show above.

### System efficiency of hydrogen production

In order to calculate system efficiency of hydrogen production, we first evaluated the steam conversion rate of our electrolysis test. The steam conversion rate can be calculated theoretically or experimentally. In theory, it can be calculated according to equation (2):

$$\frac{N_{\text{H}_2\text{O,consumed}}}{N_{\text{H}_2\text{O,input}}} \tag{2}$$

where  $N_{\text{H}_2\text{O,input}}$  is the water input which can be obtained from

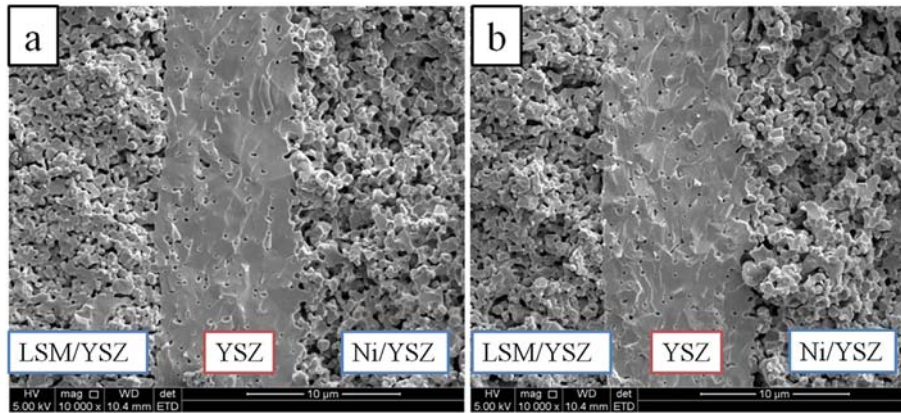


Fig. 8 – The cross-section of the single cell before (a) and after (b) electrolysis.

the peristaltic pump;  $N_{\text{H}_2\text{O,consumed}}$  is the water consumption which can be calculated via Faraday's law in the ideal condition. As a result, the theoretical steam conversion rate is generally in proportion to current density if the current efficiency (Faradic efficiency) is assumed to be 100% in the entire electrolysis process.

The experimental steam conversion rate can also be calculated in this work, based on equation (3):

$$\frac{N_{\text{H}_2\text{O,input}} - N_{\text{H}_2\text{O,condensed}}}{N_{\text{H}_2\text{O,input}}} \quad (3)$$

where  $N_{\text{H}_2\text{O,condensed}}$  is the amount of the condensed water after electrolysis. It has to be noted that the condensation was only conducted after the electrolysis becomes stable, so the value of  $N_{\text{H}_2\text{O,condensed}}$  was calculated by averaging different measurements ( $n > 3$ ). Fig. 11 shows the comparison of the experimental and theoretical values of the steam conversion rate. Apparently, the experimental data and theoretical calculations agree well in the present investigation: steam conversion rates of 12.4%, 23% and 82.2% are obtained at  $0.2 \text{ A cm}^{-2}$  for the 1-cell, 2-cell and 30-cell stacks, respectively, whereas the specific hydrogen production rates for these three stacks are 1.49, 1.4 and  $1.37 \text{ sccm/cm}^2$ , respectively, based on the measurements from the flow meter after condensing (Fig. 1). The good agreement of the theoretical

value and experimental calculation also suggests that we can obtain the energy losses related with the unreacted steam accordingly. This is an important assumption for our system efficiency calculations in the following part.

In order to simplify the electrolysis process, we introduce the thermal neutral voltage  $V_{\text{tn}}$  for our system efficiency calculation. The value of  $V_{\text{tn}}$  is defined by

$$V_{\text{tn}} = \Delta H / 2F \quad (4)$$

where  $\Delta H$  is the enthalpy change of the core electrolysis reaction, as is shown in equation (5):



$F$  represents the Faraday constant. At  $800 \text{ }^\circ\text{C}$ , the theoretical value of  $V_{\text{tn}}$  is 1.28 V. When the electrolysis voltage is higher than  $V_{\text{tn}}$ , the thermal energy produced by the current flow is greater than the thermal energy demand. On the contrary, excess thermal energy is required for electrolysis if the electrolysis voltage is lower than  $V_{\text{tn}}$ . The extra thermal energy required  $E_{\text{extra}}$  can be calculated via equation (6):

$$E_{\text{extra}} = (V_{\text{tn}} - V_e) \times i \times A \times c \quad (6)$$

where  $V_e$  denotes electrolysis voltage;  $i$  represents current density;  $A$  is the effective area for each single cell, which in our case is  $63 \text{ cm}^2$ ;  $c$  denotes the cell number in the stack.

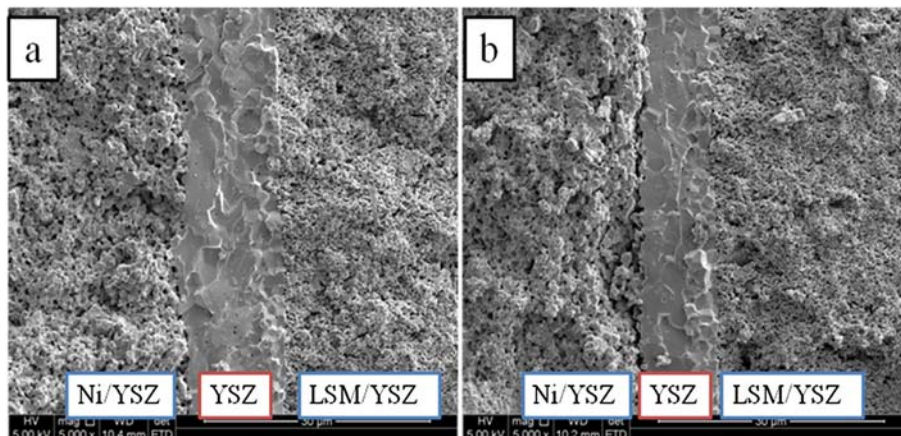


Fig. 9 – The cross-section of the bottom cell in the 2-cell stack before (a) and after (b) electrolysis.

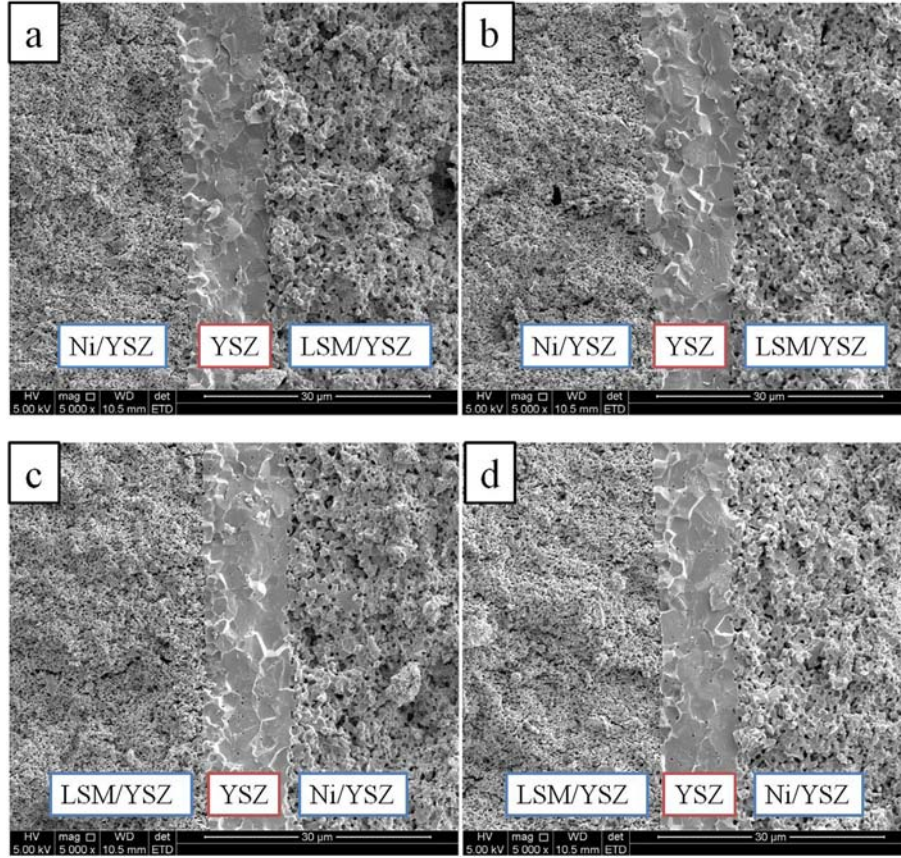


Fig. 10 – The cross-section of the top cell in the 2-cell stack before (a) and after (b), (c), (d) electrolysis.

During our electrolysis process,  $H_2$  and  $H_2O(g)$  input was preheated. We thus refer this energy demand as  $E_{\text{heat}}$ , where

$$E_{\text{Heat}} = f_{H_2O(g)} \times \int_{T_{\text{room}}}^T C_{PH_2O(g)}(T) dT + f_{H_2O(g)} \times \int_{H_2O(l)}^{H_2O(g)} \Delta H(25^\circ C) + f_{H_2} \times \int_{T_{\text{room}}}^T C_{PH_2}(T) dT \quad (7)$$

In eqn (7),  $f_{H_2O(g)}$  and  $f_{H_2}$  are the flow rates of the steam and  $H_2$ , respectively;  $C_{PH_2O(g)}$  and  $C_{PH_2}$  are the corresponding heat capacities, respectively.  $T$  represents the operating temperature, and  $T_{\text{room}}$  denotes room temperature, i.e.  $25^\circ C$ . According to thermodynamic statistics [25],  $C_{PH_2O(g)} = 30.00 + 0.01071T + 33000/T^2$ ,  $C_{PH_2} = 27.28 + 0.00326T + 50000/T^2$ . Assume electrolysis reaction is at a temperature of  $800^\circ C$  for the whole cell, and the outlet temperature of the system is  $600^\circ C$  by measurements, the energy loss,  $E_{\text{loss}}$ , before steam,  $H_2$  and  $O_2$  are exhausted can be given by:

$$E_{\text{loss}} = f'_{H_2O(g)} \times \int_{600}^{800} C_{PH_2O(g)}(T) dT + f'_{H_2} \times \int_{600}^{800} C_{PH_2}(T) dT + f'_{O_2} \times \int_{600}^{800} C_{PO_2}(T) dT \quad (8)$$

where  $f'_{H_2O(g)}$ ,  $f'_{H_2}$  and  $f'_{O_2}$  are the flow rates of steam,  $H_2$  and  $O_2$  out of the electrolysis system, respectively. The heat

capacity of oxygen can be calculated by an empirical equation  $C_{PO_2} = 29.96 + 0.00418T - 167,000/T^2$ . In our calculation, the operating conditions for the samples are listed in Table 2. According to the Faraday law, the mole number of the core reaction is:

$$n = \frac{iAC}{2F} \quad (9)$$

We assume current efficiency to be 100%, and then obtain the flow rates of  $H_2$  and  $O_2$  at the outlet accordingly. On one hand, in the case of the electrolysis voltage is lower than  $V_{\text{tn}}$ , the system efficiency can be calculated via:

$$\eta_{\text{system}} = \frac{E_{\Delta H}}{E_{\text{extra}} + E_{\text{electric}} + E_{\text{heat}} + E_{\text{loss}}} \quad (10)$$

where

$$E_{\text{electric}} = V_e \times i \times A \times c \quad (11)$$

and  $E_{\Delta H}$  is the enthalpy value of the produced hydrogen. On the other hand, in the case of the electrolysis voltage is higher than  $V_{\text{tn}}$ , the system efficiency can be calculated using:

$$\eta_{\text{system}} = \frac{E_{\Delta H}}{E_{\text{electric}} + E_{\text{heat}} + E_{\text{loss}}} \quad (12)$$

We also calculated the heat demand to heat the stacks apart from the gases and the energy required to keep the stacks at the working temperature. According to the thermodynamic statistics of the materials in the stacks [25] and the

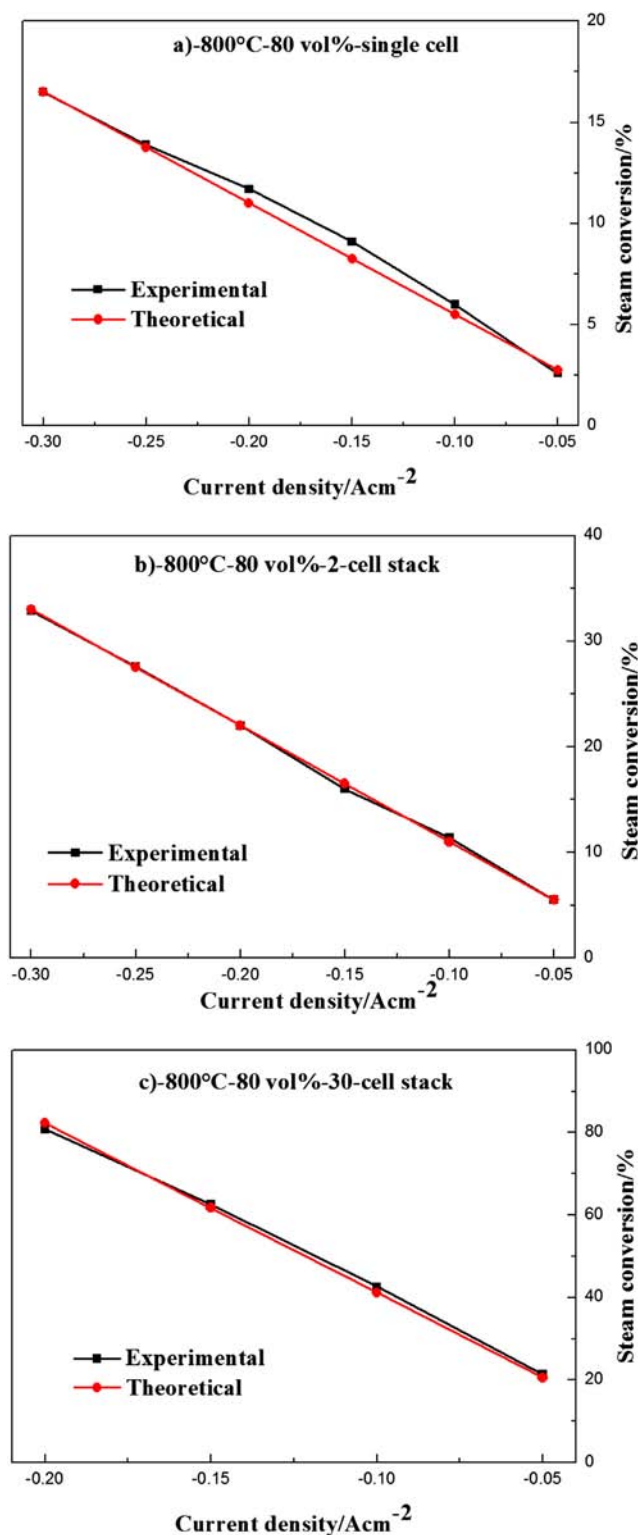


Fig. 11 – Comparison of the theoretical and experimental steam conversion rate for stacks of 1-cell (b) 2-cell (c) 30-cell.

temperature distribution inside the stacks obtained in our previous work [27], the overall heat requirement for the 1-cell stack is estimated to be 1.1 kJ. This heat requirement is negligible in comparison with the heat demand of gases.

Table 2 – Operating conditions of electrolysis for the single cell, 2-cell stack and 30-cell stack.

Conditions	Single cell	2-cell stack	30-cell stack
Electrolysis voltage and current density	1.1 V @ 0.2 A cm <sup>-2</sup>	2.3 V @ 0.2 A cm <sup>-2</sup>	40.7 V @ 0.2 A cm <sup>-2</sup>
Operating temperature	800 °C		
Steam electrode gas flow	0.8 L min <sup>-1</sup> H <sub>2</sub> O(g) and 0.2 L min <sup>-1</sup> H <sub>2</sub>		3.2 L min <sup>-1</sup> H <sub>2</sub> O(g) and 0.8 L min <sup>-1</sup> H <sub>2</sub>
Air electrode gas flow	1.5 L min <sup>-1</sup> Air		12 L min <sup>-1</sup> Air
Temperature of water supply	25 °C		

Finally, we obtained the system efficiencies for the 1-cell, 2-cell and 30-cell stacks are 16.1%, 27.2% and 52.7%, respectively. And according to equation (9), the hydrogen production rates are 0.088, 0.176 and 1.64 L min<sup>-1</sup> for the single cell, 2-cell stack, and 30-cell stack, respectively. The specific hydrogen production rates for these three stacks are thus all 1.4 sccm/cm<sup>2</sup> in accordance to our assumption, which is very close to our measurement results. It has also to be noted that the average electrolysis voltage for each repeating cell in the 30-cell stack is 1.3V which is well higher than  $V_{tm}$ . However, the average electrolysis voltage for each cell in the 1-cell and 2-cell stacks is lower than 1.2V.

According to our calculation, the system efficiency of the 30-cell stack is higher than that of the 1-cell and 2-cell stacks to a large extent. The higher average electrolysis voltage for each repeating cell in the 30-cell stack ensures an overall exothermic effect in the stack. The joule heat may cause a partial temperature increase which is favorable for the electrochemical process. Furthermore, the disproportional ASR of the 1-cell, 2-cell and 30-cell stacks also indicates the advantage of the excess heat produced by the current. Beyond the higher efficiency, the 30-cell stack test has also a much higher steam conversion rate (82.2%) in comparison with the 1-cell and 2-cell stack. In other words, the electrolysis of the 30-cell stack has a less energy loss during electrolysis. In summary, multi-cell stack system is more efficient in hydrogen production, and has higher hydrogen production rate and system efficiency if joule effect is not counted.

## Summary and conclusions

- (1) Samples of 1-cell, 2-cell and 30-cell stacks were tested in the mode of SOEC at 800 °C up to 500h without significant degradation, and achieved specific hydrogen production rates of 1.49, 1.4 and 1.37 sccm/cm<sup>2</sup>, respectively.
- (2) The 1-cell, 2-cell and 30-cell stacks obtained steam conversion rates of 12.4%, 23% and 82.2%, respectively, and system efficiencies of 16.1%, 27.2% and 52.7%, respectively.
- (3) The multi-cell stack obtains higher system efficiency than the single cell or short stack.

## Acknowledgments

The authors would like to thank the financial support from the Ningbo Natural Science Foundation (2013A610028), the Chinese Academy of Sciences (Grant No. KJCX2-YW-H21-01), and the International S&T Cooperation Program of China (2012DFA60440).

## REFERENCES

- [1] Konieczny A, Mondal K, Wiltowski T, Dydo P. Catalyst development for thermocatalytic decomposition of methane to hydrogen. *Int J Hydrogen Energy* 2008;33:264–72.
- [2] Balat Mu, Balat Me. Political, economic and environmental impacts of biomass-based hydrogen. *Int J Hydrogen Energy* 2009;34:3589–603.
- [3] Ni M, Leung MKH, Leung DYC, Sumathy K. A review and recent developments in photocatalytic water-splitting using TiO<sub>2</sub> for hydrogen production. *Renew Sustain. Energy Rev* 2007;11:401–25.
- [4] Ni M, Leung DYC, Leung MKH, Sumathy K. An overview of hydrogen production from biomass. *Fuel Process. Technol* 2006;87:461–72.
- [5] Steinfeld A. Solar thermochemical production of hydrogen—a review. *Sol Energy* 2005;78:603–15.
- [6] Fishcher M. Review of hydrogen production with photovoltaic electrolysis systems. *Int J Hydrogen Energy* 1986;11:495–501.
- [7] Fujiwara S, Kasai H, Yamauchi K, Yamada S, Makino K, Matsunaga M, et al. Hydrogen production by high temperature electrolysis with nuclear reactor. *Prog Nucl Energy* 2008;50:422–6.
- [8] Brisse A, Schefold J, Zahid M. High temperature water electrolysis in solid oxide cells. *Int J Hydrogen Energy* 2008;33:5375–82.
- [9] Laguna-Bercero MA, Skinner SJ, Kilner JA. Performance of solid oxide electrolysis cells based on Scandia stabilized zirconia. *J Power Sources* 2009;192:126–31.
- [10] Laguna-Bercero MA, Campana R, Larrea A, Kilner JA, Orera VM. Electrolyte degradation in anode supported microtubular yttria stabilized zirconia-based solid oxide steam electrolysis cells at high voltages of operation. *J Power Sources* 2011;196:8942–7.
- [11] Schefold J, Brisse A, Zahid M. Electronic conduction of yttria-stabilized zirconia electrolyte in solid oxide cells operated in high temperature water electrolysis. *J Electrochem. Soc* 2009;156:B897–904.
- [12] Kim S, Yu J, Seo D, Han I, Woo S. Hydrogen production by high temperature electrolysis using solid oxide electrolyzer cells. *ECS Trans* 2011;35:2957–60.
- [13] Knibbe R, Traulsen ML, Hauch A, Ebbesen SD, Mogensen M. Solid oxide electrolysis cells: degradation at high current densities. *J Electrochem. Soc* 2010;157:B1209–17.
- [14] Minh NQ. Development of reversible solid oxide fuel cell (RSOFC) cells and stacks. *ECS Trans* 2011;35:2897–904.
- [15] Hauch A, Ebbesen SD, Jensen SH, Mogensen M. Solid oxide electrolysis cells: microstructure and degradation of the Ni/Yttria-stabilized zirconia electrode. *J Electrochem. Soc* 2008;155:B1184–93.
- [16] Stephen Herring J, O'Brien James E, Hartvigsen Joseph J. Progress in high-temperature electrolysis for hydrogen production using planar SOFC technology. *Int J Hydrogen Energy* 2007;32:440–50.
- [17] Ebbesen Sune Dalgaard, Høgh Jens, Nielsen Karsten Agersted, Nielsen Jens Ulrik, Mogensen Mogens. Durable SOC stacks for production of hydrogen and synthesis gas by high temperature electrolysis. *Int J Hydrogen Energy* 2011;36:7363–73.
- [18] Kim S, Yu J-Y, Seo D-W, Han I-S, Woo S-K. Hydrogen production performance of 3-cell flat-tubular solid oxide electrolysis stack. *Int J Hydrogen Energy* 2012;37:78–83.
- [19] Ni Meng, Leung Michael KH, Leung Dennis YC. Energy and exergy analysis of hydrogen production by solid oxide steam electrolyzer plant. *Int J Hydrogen Energy* 2007;32:4648–60.
- [20] Wang Zhenwei, Mori Masashi, Araki Takuto. Steam electrolysis performance of intermediate-temperature solid oxide electrolysis cell and efficiency of hydrogen production system at 300 N m<sup>3</sup> h<sup>-1</sup>. *Int J Hydrogen Energy* 2010;35:4451–8.
- [21] Zhang Wenqiang, Yu Bo, Xu Jingming. Efficiency evaluation of high-temperature steam electrolytic systems coupled with different nuclear reactors. *Int J Hydrogen Energy* 2012;37:12060–8.
- [22] Liu Mingyi, Yu Bo, Xu Jingming. System efficiency of solid oxide steam electrolysis. *Journal of Tsinghua University*; 2009. pp. 868–71.
- [23] Li Tingshuai, Chen Tao, Miao He, Wang Weiguo, Xu Cheng. Effect of reduction temperature on the electrochemical properties of a Ni/YSZ anode-supported solid oxide fuel cell. *J Alloys Compd* 2010;495:138–43.
- [24] Zheng Yifeng, Li Qingshan, Guan Wanbin, Xu Cheng, Wu Wei, Guo Wang Wei. Investigation of 30-cell solid oxide electrolyzer stack modules for hydrogen production. *Ceramics International* 2014;40:5801–9.
- [25] HSC chemistry, chemistry software, Houston, TX.
- [26] Dasari Hari Prasad, Park Sun-Young, Kim Jeonghee, Lee Jong-Ho, Kim Byung-Kook, Je Hae-June, et al. Electrochemical characterization of Ni-yttria stabilized zirconia electrode for hydrogen production in solid oxide electrolysis cells. *J Power Sources* 2013;240:721–8.
- [27] Guan WB, Zhai HJ, Jin L, Xu C, Wang WG. Temperature measurement and distribution inside planar SOFC stacks. *Fuel cells* 2012;12(1):24–31.